Evolution from helical to collinear ferromagnetic order of the Eu^{2+} spins in $RbEu(Fe_{1-x}Ni_x)_4As_4$

Qianhui Xu,[1,*] Yi Liu,[2,3,*] Sijie Hao,[4,*] Jiahui Qian,[5] Cheng Su,[1] Chin-Wei Wang,[6] Thomas Hansen,[7] Zhendong Fu,[8] Yixi Su,[9] Wei Li,[5] Guang-Han Cao,[3,†] Yinguo Xiao,[10,‡] and Wentao Jin[1,§]

[1]*School of Physics, Beihang University, Beijing 100191, China*
[2]*College of Science, Zhejiang University of Technology, Hangzhou 310023, China*
[3]*Department of Physics, Zhejiang University, Hangzhou 310027, China*
[4]*Department of Physics, Beijing Normal University, Beijing 100875, China*
[5]*State Key Laboratory of Surface Physics and Department of Physics, Fudan University, Shanghai 200433, China*
[6]*National Synchrotron Radiation Research Center, Hsinchu 30077, Taiwan*
[7]*Institut Laue-Langevin, Boîte Postale 156, 38042 Grenoble Cedex 9, France*
[8]*Neutron Platform, Songshan Lake Materials Laboratory, Dongguan 523808, China*
[9]*Jülich Centre for Neutron Science JCNS at Heinz Maier-Leibnitz Zentrum (MLZ), Forschungszentrum Jülich GmbH, Lichtenbergstraße 1, D-85747 Garching, Germany*
[10]*School of Advanced Materials, Shenzhen Graduate School, Peking University, Shenzhen 518055, China*

(Received 31 August 2021; revised 28 November 2021; accepted 13 January 2022; published 31 January 2022)

The ground-state magnetic structures of the Eu^{2+} spins in recently discovered $RbEu(Fe_{1-x}Ni_x)_4As_4$ superconductors have been investigated by neutron powder diffraction measurements. It is found that as the superconductivity gets suppressed with the increase in Ni doping, the magnetic propagation vector of the Eu sublattice diminishes, corresponding to the decrease in the rotation angle between the moments in neighboring Eu layers. The ferromagnetic Eu layers are helically modulated along the c axis with an incommensurate magnetic propagation vector in both the ferromagnetic superconductor $RbEu(Fe_{0.95}Ni_{0.05})_4As_4$ and the superconducting ferromagnet $RbEu(Fe_{0.93}Ni_{0.07})_4As_4$. Such a helical structure transforms into a purely collinear ferromagnetic structure for nonsuperconducting $RbEu(Fe_{0.91}Ni_{0.09})_4As_4$, with all the Eu^{2+} spins lying along the tetragonal (1 1 0) direction. The evolution from helical to collinear ferromagnetic order of the Eu^{2+} spins with increasing Ni doping is supported by first-principles calculations. The variation of the rotation angle between adjacent Eu^{2+} layers can be well explained by considering the change of magnetic exchange couplings mediated by the indirect Ruderman-Kittel-Kasuya-Yosida interaction.

DOI: 10.1103/PhysRevResearch.4.013077

I. INTRODUCTION

The discovery of iron-based superconductors in 2008 has stimulated worldwide research interests in the investigations of the interplay between magnetism and unconventional superconductivity in these novel materials [1,2]. Among various members of the iron-based superconductors, the ternary "$EuFe_2As_2$" (Eu122) system is a unique representative and has attracted much attention due to the existence of two magnetic sublattices in the unit cell and the strong coupling between spin, lattice, and charge degrees of freedom [3–5]. The undoped parent compound $EuFe_2As_2$ shows an A-type antiferromagnetic (AFM) order of the localized Eu^{2+} spins below 19 K, in addition to the spin-density-wave (SDW) order of the itinerant Fe moments below 190 K [6,7]. By suppressing the SDW order in the Fe sublattice, superconductivity can be achieved by means of chemical substitutions or applying external pressure [3,8,9]. In the superconducting ground state, single-crystal neutron diffraction or x-ray resonant magnetic scattering experiments have confirmed that strong ferromagnetism from Eu $4f$ orbitals with an ordered moment of $\sim 7\,\mu_B$ per Eu atom can coexist microscopically with bulk superconductivity and reach a compromise [10–14]. The intriguing coexistence of ferromagnetism and superconductivity revealed in the Eu122 system drives the experimental efforts to further explore other novel Eu-containing iron-based superconductors.

In 2016, superconductivity with the transition temperature (T_{SC}) of approximately 31–36 K was discovered in a new family of iron pnictides $CaAFe_4As_4$ and $SrAFe_4As_4$ (A = K, Rb, and Cs) possessing the "1144" -type structure [15]. Later on, $RbEuFe_4As_4$ (denoted as Eu1144 below), crystallizing as an intergrowth structure of heavily hole-doped superconducting $RbFe_2As_2$ ($T_{SC} = 2.6$ K) [16] and nonsuperconducting $EuFe_2As_2$, was reported to be a superconductor as well with

*These authors contributed equally to this work.
†ghcao@zju.edu.cn
‡y.xiao@pku.edu.cn
§wtjin@buaa.edu.cn

$T_{SC} = 36$ K [17,18]. The FeAs layers in Eu1144 are intrinsically hole doped due to the charge homogenization associated with the structural hybridization, which is responsible for the absence of Fe-SDW order and the occurrence of superconductivity. Ascribing to the longer interlayer distance between the Eu layers in Eu1144 compared to Eu122, the Eu^{2+} spins order magnetically at a lower temperature of $T_m = 15$ K.

Based on the magnetization and specific-heat data obtained from high-quality powder samples, $RbEuFe_4As_4$ was speculated to be a ferromagnetic superconductor with a robust coexistence of superconductivity and ferromagnetism [17]. Neutron diffraction measurements on a Eu1144 single crystal have been performed to clarify how the two-dimensional ferromagnetic Eu layers stack along the c axis [19]. A magnetic propagation vector of $k = (0, 0, 0.25)$ is revealed, suggesting the rotation angle of 90° between the in-plane ferromagnetically aligned Eu^{2+} spins on adjacent layers. Such a helical magnetic structure of undoped Eu1144 is in stark contrast to the collinear A-type AFM structure of undoped $EuFe_2As_2$ but resembles those of $EuCo_2As_2$ and $EuNi_2As_2$, showing an incommensurate magnetic propagation vector of $k = (0, 0, 0.79)$ and $k = (0, 0, 0.92)$, respectively [20,21].

By introducing extra itinerant electrons via the substitution of Ni^{2+} ($3d^8$) for Fe^{2+} ($3d^6$), the intrinsically doped hole carriers in $RbEuFe_4As_4$ can be compensated. Systematic macroscopic characterizations including resistivity, magnetization, and specific-heat measurements have been performed on polycrystalline and single-crystal samples of $RbEu(Fe_{1-x}Ni_x)_4As_4$ to establish the superconducting and magnetic phase diagram [22,23]. It is figured out that T_{SC} decreases rapidly with the Ni doping, whereas the magnetic ordering temperature of the Eu sublattice T_m remains essentially unchanged. Consequently, $RbEu(Fe_{1-x}Ni_x)_4As_4$ transforms from the ferromagnetic superconductor with $T_{SC} > T_m$ for $x < 0.07$, to the so-called "superconducting ferromagnet" (SFM) with $T_m > T_{SC}$ for $0.07 \leqslant x \leqslant 0.08$ and finally to the ferromagnetic nonsuperconductor for $x > 0.09$. Furthermore, a recovered Fe-AFM state is proposed for $0.04 \leqslant x \leqslant 0.10$ based on the resistivity data on polycrystalline samples [22].

As the helical magnetic order of the Eu^{2+} spins with a two-dimensional (2D) character in undoped Eu1144 is proposed to be associated with the presence of superconductivity [24,25], it is of great interest to clarify how the magnetic structure of $RbEu(Fe_{1-x}Ni_x)_4As_4$ develops against the weakening of the superconductivity induced by Ni doping. Fitting to the magnetic susceptibility in the paramagnetic state yields comparable positive values of Curie-Weiss temperature for samples with different x values [22,23], reflecting dominant in-plane ferromagnetic interactions between the Eu^{2+} moments. Detailed neutron diffraction measurements on $RbEu(Fe_{1-x}Ni_x)_4As_4$ will deliver important information regarding how the stacking pattern of the ferromagnetic Eu layer along the c-axis changes with x, and how it will be correlated with the suppression of superconductivity.

Here we present a systematic study of the magnetic structures of Ni-doped Eu1144 with different doping levels as determined by neutron powder diffraction (NPD). We find that as the superconductivity gets suppressed gradually with the increase in Ni doping, the magnetic propagation vector of the Eu sublattice diminishes, corresponding to the decrease in the rotation angle between the moments in neighboring Eu layers. No evidence of the proposed recovery of Fe-SDW order is observed within our experimental resolution. The variation of the rotation angle between adjacent Eu^{2+} layers can be well explained by considering the change in magnetic exchange couplings mediated by the indirect Ruderman-Kittel-Kasuya-Yosida (RKKY) interaction.

II. EXPERIMENTAL DETAILS AND CALCULATION METHODS

Polycrystalline samples of $RbEu(Fe_{1-x}Ni_x)_4As_4$ ($x = 0.05$, 0.07, 0.09) of ~4 g were synthesized by the solid-state reaction method as described in Ref. [22]. The phase purity was checked by x-ray diffraction on a PANalytical x-ray diffractometer with a monochromatic Cu $K\alpha_1$ radiation. The doping concentration of Ni in three samples was checked by energy-dispersive x-ray spectroscopy to be 5.6(6)%, 7.1(8)%, and 8.9(5)%, respectively, well consistent with the nominal values. A small amount of FeAs impurity was found to exist in the samples with $x = 0.05$ and 0.07, and small amounts of $RbFe_2As_2$ and $EuFe_2As_2$ impurities were identified in the sample with $x = 0.09$. Low-temperature NPD measurements on the samples with $x = 0.05$ were performed on the high-intensity powder diffractometer Wombat [26] at the OPAL facility (Lucas Height, Australia) using incident neutrons with the wavelength of 2.41 and 1.54 Å, whereas the data of the sample with $x = 0.07$ were collected using the wavelength of 1.54 Å only. NPD measurements on the sample with $x = 0.09$ were performed on the high-intensity powder diffractometer D20 at Institut Laue-Langevin (Grenoble, France) using incident neutrons with the wavelength of 2.41 and 1.30 Å. In order to minimize the effect of neutron absorption by the Eu atoms, we have filled the powder samples into the double-wall hollow vanadium cylinder. Refinements of both nuclear and magnetic structures were carried out using the FULLPROF program suite [27].

The first-principles calculations presented in this paper are performed using the projected augmented-wave method [28] as implemented in the VASP code [29]. The exchange-correlation potential is calculated using the generalized gradient approximation (GGA) as proposed by Perdew *et al.* [30]. We have included the strong Coulomb repulsion in the Eu-4f orbitals on a mean-field level using the GGA + U_{eff} approximation. Since there exist no spectroscopy data for $RbEu(Fe_{1-x}Ni_x)_4As_4$, we have used a U_{eff} of 8 eV throughout this paper, which is the standard value for an Eu^{2+} ion [12,13,31]. The results have been checked for consistency with varying U_{eff} values. U_{eff} is not applied to the itinerant Fe-3d and Ni-3d orbitals. Additionally, the spin-orbit coupling is included for all atoms with the second variational method in the calculations. These calculations are performed using the experimental crystal structure as determined by the neutron diffraction measurements.

III. RESULTS

The ground-state magnetic structures of the Eu^{2+} spins in $RbEu(Fe_{1-x}Ni_x)_4As_4$ with different Ni-doping levels

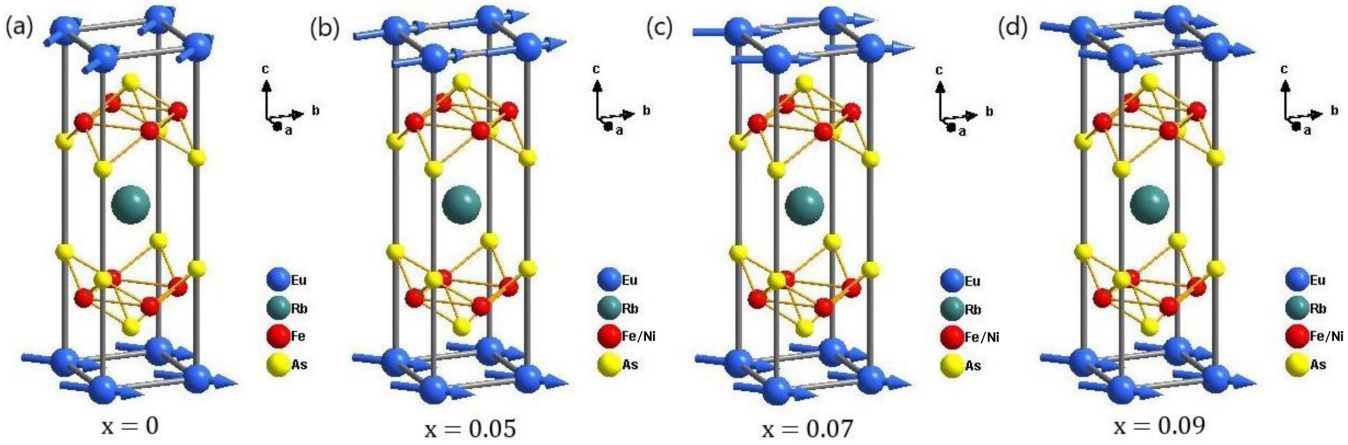

FIG. 1. The ground-state magnetic structure of $RbEu(Fe_{1-x}Ni_x)_4As_4$ with (a) $x = 0$ [19], (b) $x = 0.05$, (c) $x = 0.07$, and (d) $x = 0.09$ in which the rotation angle between the in-plane ferromagnetically aligned Eu^{2+} moments on adjacent layers are 90°, ∼49°, ∼26°, and 0°, respectively.

($x = 0.05$, 0.07, and 0.09) are determined by NPD measurements and illustrated in Figs. 1(b)–1(d) together with the helical magnetic structure of undoped $RbEuFe_4As_4$ ($x = 0$) with $k = (0, 0, 0.25)$ [Fig. 1(a)] as determined in Ref. [19], which will be discussed in detail below.

Figure 2 shows the NPD patterns of $RbEu(Fe_{0.95}Ni_{0.05})_4As_4$ at 20 and 3.9 K. According to the superconducting and magnetic phase diagram of $RbEu(Fe_{1-x}Ni_x)_4As_4$ deduced from macroscopic measurements in Ref. [22] for this composition, the temperature of 20 K is above $T_m (= 15\ \text{K})$ but below $T_{SDW} (= 28.9\ \text{K})$, which is the SDW ordering temperature of Fe. As shown in Figs. 2(a) and 2(c), the diffraction patterns at 20 K can be well fitted with the crystal structure reported in Ref. [22] (space group $P4/mmm$) with a small amount of FeAs impurity (7% wt). Within our experimental uncertainty, no magnetic reflections at (0.5, 0.5, 3) ($Q = 1.84\ \text{Å}^{-1}$) associated with possible Fe-AFM order can be identified, assuming that the Fe^{2+} moments order in the hedgehog spin-vortex crystal (SVC) motif in each Fe plane and are antiferromagnetically stacked along the c direction, similar to that observed in isostructural $CaK(Fe_{1-x}Ni_x)_4As_4$ [32,33].

Upon cooling down to 3.9 K, which is well below T_m, the magnetic reflections due to the magnetic ordering of Eu appear as satellite peaks close to the nuclear reflections. As shown in Fig. 2(d), the incident neutron wavelength

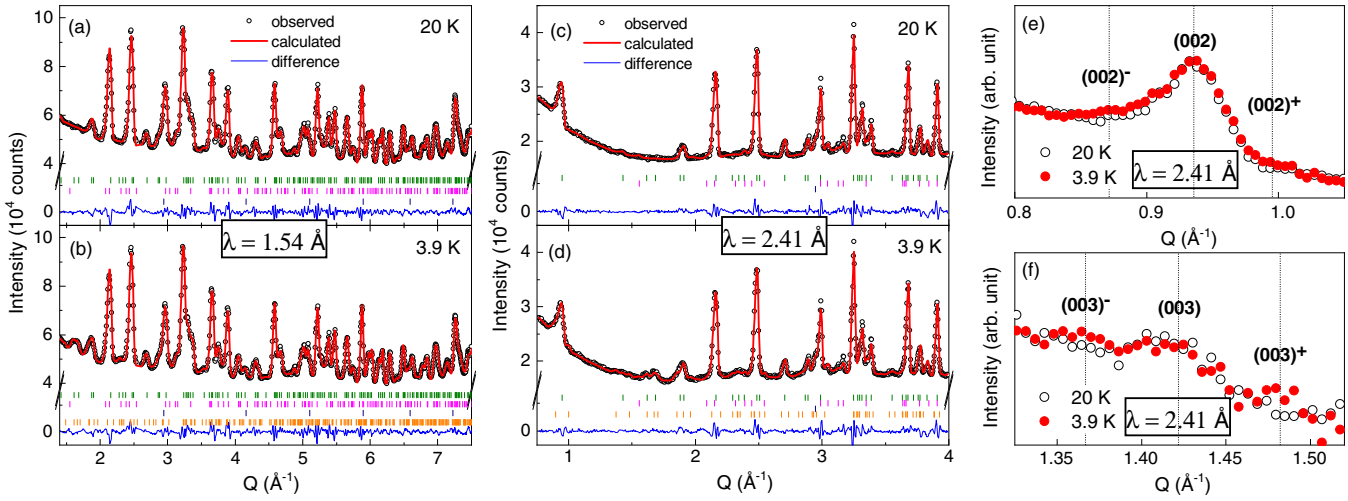

FIG. 2. NPD patterns of $RbEu(Fe_{0.95}Ni_{0.05})_4As_4$ at [(a) and (c)] 20 K and [(b) and (d)] 3.9 K and the Rietveld refinements. The left (a) and (b) and right (c)–(f) panels show the data collected using the incident neutron wavelength of 1.54 and 2.41 Å, respectively. The patterns in (b) and (d) are the refinement results obtained by adopting a magnetic structure model with the irreducible representation Γ_5 as described in the text. The circles represent the observed intensities, and the solid lines are the calculated patterns. The differences between the observed and calculated intensities are shown at the bottom. The vertical bars in olive, magenta, navy, and orange colors indicate the expected nuclear Bragg reflections from the $RbEu(Fe_{0.95}Ni_{0.05})_4As_4$ main phase, FeAs impurity, vanadium sample container, and the magnetic Bragg reflections from $RbEu(Fe_{0.95}Ni_{0.05})_4As_4$, respectively. (e) and (f) show the enlarged high-resolution diffraction patterns at 3.9 and 20 K around the (0 0 2) and (0 0 3) nuclear peak positions, respectively, visualizing the incommensurate magnetic satellite reflections appearing at 3.9 K.

TABLE I. Refined results for the nuclear and magnetic-structure parameters of $RbEu(Fe_{1-x}Ni_x)_4As_4$ with $x = 0.05$, 0.07 and 0.09. The atomic positions are as follows: Eu, 1*a* (0, 0, 0); Rb, 1*d* (0.5, 0.5, 0.5); Fe/Ni, 4*i* (0, 0.5, z_{Fe}); As1, 2*g* (0, 0, z_{As1}); As2, 2*h* (0.5, 0.5, z_{As2}). The occupancies of Fe and Ni were fixed according to the nominal compositions, respectively. The nuclear structure parameters and the scale factor derived from the refinement of 20 K data were fixed in the magnetic-structure refinements (space group: $P4/mmm$).

Composition		$RbEu(Fe_{0.95}Ni_{0.05})_4As_4$		$RbEu(Fe_{0.93}Ni_{0.07})_4As_4$		$RbEu(Fe_{0.91}Ni_{0.09})_4As_4$	
Temperature		20 K	3.9 K	20 K	3.3 K	20 K	2 K
Eu	B_{iso} (Å^2)	1.3(1)		1.2(1)		0.22(5)	
	M (μ_B)		6.3(2)		6.3(2)		6.5(1)
Rb	B_{iso} (Å^2)	1.4(1)		1.3(1)		1.1(1)	
Fe/Ni	z_{Fe}	0.2309(2)		0.2310(2)		0.2315(1)	
	B_{iso} (Å^2)	1.0(1)		0.8(1)		0.26(1)	
As1	z_{As1}	0.3344(4)		0.3339(4)		0.3339(2)	
	B_{iso} (Å^2)	1.1(1)		0.8(1)		0.24(3)	
As2	z_{As2}	0.1263(4)		0.1263(4)		0.1277(2)	
	B_{iso} (Å^2)	1.3(1)		0.8(1)		0.24(3)	
	a (Å)	3.8652(4)	3.8651(2)	3.8649(5)	3.8646(2)	3.8921(3)	3.8920(2)
	c (Å)	13.117(2)	13.117(1)	13.109(2)	13.108(1)	13.218(1)	13.216(1)
	R_{F^2}	1.29	1.28	1.31	1.34	1.86	2.01
	R_{wF^2}	1.73	1.72	1.83	1.86	2.40	2.63
	R_F	0.43	0.44	0.42	0.43	0.36	0.36

of $\lambda = 2.41$ Å provides a better resolution at the low-Q region, confirming the incommensurate nature of the magnetic peaks. The magnetic reflections at $(002)^-/(002)^+$ and $(003)^-/(003)^+$ emerge in both sides of the (0 0 2) and (0 0 3) peaks as illustrated in Figs. 2(e) and 2(f). Using the K_SEARCH program integrated in the FULLPROF suite, the magnetic propagation vector of $k = (0, 0, 0.136(4))$ is figured out for $RbEu(Fe_{0.95}Ni_{0.05})_4As_4$.

According to the representation analysis performed using the BASIREPS program also integrated in the FULLPROF suite (see Appendix B for details) for the space group of $P4/mmm$, only two magnetic representations are possible for the Eu(1*a*) site with the propagation vector of $k = (0, 0, 0.136(4))$, which we label as Γ_1 and Γ_5, respectively. Γ_1 allows the *c*-axis aligned ferromagnetic Eu layers stacking with modulated moment size values at different layers, which

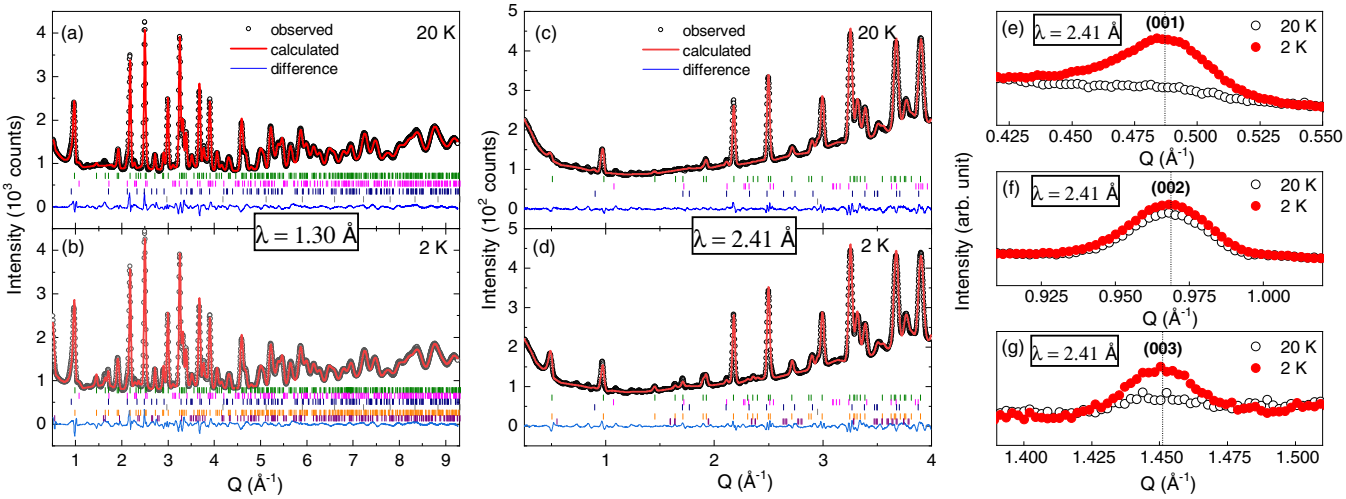

FIG. 3. NPD patterns of $RbEu(Fe_{0.91}Ni_{0.09})_4As_4$ at [(a) and (c)] 20 K and [(b) and (d)] 2 K and the Rietveld refinements. The left (a) and (b) and right (c)–(g) panels show the data collected using the incident neutron wavelengths of 1.30 and 2.41 Å, respectively. The patterns in (b) and (d) are the refinement results obtained by adopting a magnetic structure model with the irreducible representation Γ_9 as described in the text. The circles represent the observed intensities, and the solid lines are the calculated patterns. The differences between the observed and the calculated intensities are shown at the bottom. The vertical bars in olive, magenta, navy, gray, orange, and purple colors indicate the expected nuclear Bragg reflections from the $RbEu(Fe_{0.91}Ni_{0.09})_4As_4$ main phase, $EuFe_2As_2$ impurity, $RbFe_2As_2$ impurity, vanadium sample container, as well as the magnetic Bragg reflections from the $RbEu(Fe_{0.91}Ni_{0.09})_4As_4$ main phase and the $EuFe_2As_2$ impurity, respectively. (e)–(g) show the enlarged high-resolution diffraction patterns at 2 and 20 K around the (0 0 1), (0 0 2), and (0 0 3) nuclear peak positions, respectively, illustrating the commensurate magnetic contributions with $k = 0$ at 2 K.

is not consistent with the easy-plane magnetization as revealed from the single-crystal sample with a similar Ni-doping level [23]. On the other hand, Γ_5 allows the in-plane aligned ferromagnetic Eu layers to stack helically along the c axis with a constant moment size value at different layers. This model fits pretty well to the diffraction patterns at 3.9 K as shown by the solid curves in Figs. 2(b) and 2(d). As a comparison between the fitting using Γ_5 and Γ_1, Fig. 8 in Appendix B shows a better agreement of Γ_5 with the observed intensities in the very low-Q region where the magnetic form factor dominates. The nuclear structure parameters and the scale factor derived from the refinement of 20 K data was fixed in the refinement of 3.9 K data to derive the moment size of Eu to be 6.3(2) μ_B as listed in Table I. As illustrated in Fig. 1(b), the Eu^{2+} moments form an incommensurate helical structure with the moment direction lying on the ab plane but rotating by ~49° around the c axis with respect to adjacent Eu layers. Using the Bilbao Crystallographic Server [34], the magnetic space group of this helical structure is determined to be $Pm'm'm$ (No. 47.252).

Figure 3 shows the NPD patterns of RbEu$(Fe_{0.91}Ni_{0.09})_4As_4$ at 20 and 2 K. This sample is nonsuperconducting as evidenced from previous macroscopic characterizations [22]. It undergoes the magnetic ordering of the Eu sublattice at T_m (= 14.7 K) and a possible recovered Fe-SDW ordering at T_{SDW} (=31.3 K). Similar to the case of $x = 0.5$ presented above, no visible change in intensities at (0.5, 0.5, 1) ($Q = 1.25$ Å^{-1}) and (0.5, 0.5, 3) ($Q = 1.84$ Å^{-1}) associated with the Fe-AFM order can be resolved at 20 K compared with 40 K (data of which are not shown). The diffraction patterns at 20 K can be well fitted using the nuclear crystal structure in the space group of $P4/mmm$ together with small amount impurities phases of $RbFe_2As_2$ (6.2% wt) and $EuFe_2As_2$ (4.4% wt) as shown in Figs. 3(a) and 3(c).

In stark contrast to the magnetic satellite peaks displayed in RbEu$(Fe_{0.95}Ni_{0.05})_4As_4$ arising from the helical magnetic structure of Eu, here at 2 K, well below T_m, the magnetic scatterings due to the ordering of Eu^{2+} spins appear on top of the nuclear reflections for RbEu$(Fe_{0.91}Ni_{0.09})_4As_4$, which is shown in Figs. 3(e)–3(g) for (e) $Q = (0\ 0\ 1)$, (f) (0 0 2), and (g) (0 0 3) measured with a high resolution using $\lambda = 2.41$ Å. This clearly indicates a magnetic propagation vector of $k = 0$.

Magnetic representation analysis for $k = 0$ for the space group of $P4/mmm$ yields only two possible irreducible representations for the Eu(1a) site (see Appendix B for details), labeled as Γ_8 and Γ_9, respectively. They correspond to the collinear ferromagnetic structures in which all the Eu^{2+} moments are aligned along the c axis and on the ab plane, respectively. Although no magnetization data on single-crystal RbEu$(Fe_{0.91}Ni_{0.09})_4As_4$ are available, the moment direction of Eu^{2+} spins can still be identified according to the nature of magnetic neutron diffraction. As the magnetic scattering is only sensitive to the component of the moment perpendicular to Q, dramatic enhancements of intensities of (0 0 L) peaks and no visible changes in (H K 0) peak intensities suggest that the Eu^{2+} moments are mostly lying on the ab plane so that the magnetic structure model described by Γ_8 can be excluded. Indeed the Γ_9 model with all spins aligned along the in-plane (1 1 0) direction fits the diffraction patterns at 2 K quite well as shown by the solid curves in Figs. 3(b) and 3(d). As the

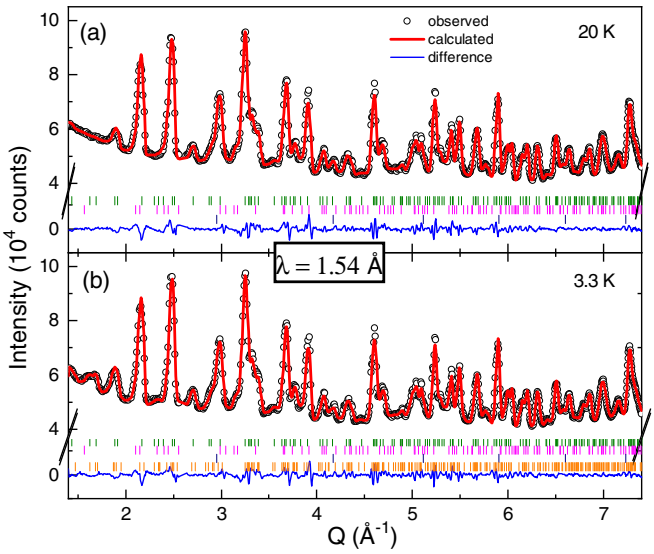

FIG. 4. NPD patterns of RbEu$(Fe_{0.93}Ni_{0.07})_4As_4$ at (a) 20 K and (b) 3.3 K collected using the incident neutron wavelength of 1.54 Å and the Rietveld refinements. The pattern in (b) is the refinement result obtained by adopting a magnetic-structure model with the irreducible representation Γ_5 as described in the text. The circles represent the observed intensities, and the solid lines are the calculated patterns. The differences between the observed and the calculated intensities are shown at the bottom. The vertical bars in olive, magenta, navy, and orange colors indicate the expected nuclear Bragg reflection from RbEu$(Fe_{0.93}Ni_{0.07})_4As_4$, FeAs impurity, vanadium sample container, and the magnetic Bragg reflection from RbEu$(Fe_{0.93}Ni_{0.07})_4As_4$, respectively.

fraction of the $EuFe_2As_2$ impurity phase is quite small (4.4% wt), including its magnetic phase into the refinement has no visible effect on the fitting of the 2 K data and the results about the 1144 main phase. Fixing the nuclear structure parameters and the scale factor derived from the refinement of 20 K data, the refinement of 2 K data yields the moment size of Eu to be 6.5(1) μ_B (see Table I). Please note that a lower saturated moment of 6.0 μ_B/Eu for $x = 0.09$ in Ref. [22] is because of some nonmagnetic Eu_2O_3 impurities forming in older samples due to oxidation of metallic Eu. In fact, the saturated moment of Eu^{2+} spins should be independent of the Ni-doping level. The magnetic structure of RbEu$(Fe_{0.91}Ni_{0.09})_4As_4$ is illustrated in Fig. 1(d). Compared with the undoped Eu1144 and RbEu$(Fe_{0.95}Ni_{0.05})_4As_4$ with $x = 0.05$, the rotation angle between the moments in neighboring Eu layers diminishes to zero for RbEu$(Fe_{0.91}Ni_{0.09})_4As_4$ with $x = 0.09$, forming a collinear in-plane ferromagnetic structure. The magnetic space group of this collinear structure is determined to be $Cmm'm'$ (No. 65.486).

After presenting the results of RbEu$(Fe_{1-x}Ni_x)_4As_4$ with $x = 0.05$ and 0.09, we come to the magnetic structure determination of the SFM RbEu$(Fe_{0.93}Ni_{0.07})_4As_4$ (T_{SC} = 11.2 K) with T_m and T_{SDW} being 15.1 and 35.0 K, respectively [22]. As shown in Fig. 4(a), the diffraction pattern of RbEu$(Fe_{0.93}Ni_{0.07})_4As_4$ at 20 K can be well fitted with the nuclear crystal structure in the space group of $P4/mmm$ together with a small amount impurities phase of FeAs (5.9% wt). Again, no magnetic peaks at (0.5, 0.5, 3) arising from

TABLE II. Energetic properties of the different spin configurations of the Eu^{2+} moments for $RbEuFe_4As_4$. The results are the total energy difference per Eu atom. The helical, antiparallel, and parallel configurations correspond to the magnetic structures in which the in-plane ferromagnetic Eu^{2+} moments on adjacent layers are vertical, antiparallel, and parallel, respectively.

Configurations	ΔE (meV)	M_{Eu} (μ_B)
Helical [$k = (0, 0, 0.25)$]	0	6.986
Antiparallel	49.71	6.962
Parallel	49.21	6.962

the Fe-AFM order can be identified. Upon cooling down to the base temperature of 3.3 K, the magnetic scattering due to magnetic ordering of Eu^{2+} spins sets in. Unfortunately the high-resolution datasets with $\lambda = 2.41$ Å are lacking for this sample due to the limited neutron beam time. However, by setting the magnetic propagation vector k itself as a variable parameter in the refinement of 3.3 K data, the diffraction pattern can be fitted pretty well with k finally converged to [0, 0, 0.071(7)] and the moment size of Eu^{2+} spins being $6.3(2)\,\mu_B$ as shown in Table I and Fig. 4(b). This result corresponds to a helical magnetic structure similar to that of $RbEu(Fe_{0.95}Ni_{0.05})_4As_4$ but with a smaller helix rotation angle of $\sim 26^\circ$.

Using first-principles calculations, the energetic properties of different spin configurations of the Eu^{2+} moments are computed for $RbEuFe_4As_4$ and $RbEu(Fe_{0.875}Ni_{0.125})_4As_4$, respectively. As shown in Tables II and III, it is found that the noncollinear helical structure with $k = (0, 0, 0.25)$ possesses the lowest energy for the parent compound $RbEuFe_4As_4$, whereas the collinear ferromagnetic structure with the Eu^{2+} moments lying on the *ab* plane is energetically favorable for $RbEu(Fe_{0.875}Ni_{0.125})_4As_4$ with $x = 0.125$. These are well consistent with our experimental findings that the rotation angle between the moments in neighboring Eu layers diminishes with increasing Ni doping and the helical structure finally transforms into a purely collinear ferromagnetic structure.

IV. DISCUSSION AND CONCLUSION

As shown in Fig. 1, the magnetic structure of the Eu^{2+} moments in $RbEu(Fe_{1-x}Ni_x)_4As_4$ undergoes a smooth evolution from the helical structure in which the in-plane ferromagnetically aligned Eu^{2+} spins on adjacent layers rotate by 90°

TABLE III. Energetic properties of the different spin configurations of the Eu^{2+} moments for $RbEu(Fe_{0.875}Ni_{0.125})_4As_4$. The results are the total energy difference per Eu atom. The helical, antiparallel, and parallel configurations correspond to the magnetic structures in which the in-plane ferromagnetic Eu^{2+} moments on adjacent layers are vertical, antiparallel, and parallel, respectively.

Configurations	ΔE (meV)	M_{Eu} (μ_B)
Helical [$k = (0, 0, 0.25)$]	0	6.971
Antiparallel	2.01	6.965
Parallel	−2.04	6.970

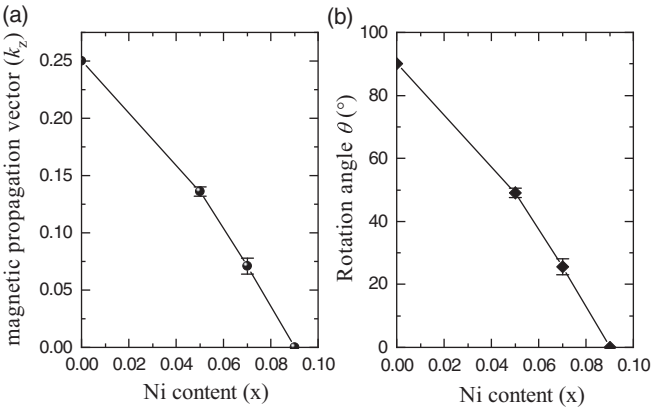

FIG. 5. The evolution of magnetic propagation vector (a) $k = (0, 0, k_z)$ and (b) the rotation angle (θ) of the Eu^{2+} spins between adjacent Eu layers in $RbEu(Fe_{1-x}Ni_x)_4As_4$ as a function of the Ni content x.

gradually to a collinear ferromagnetic structure in which all the Eu^{2+} spins point along the tetragonal (1 1 0) direction. The c component of the magnetic propagation vector k_z and the helix rotation angle (θ) are plotted in Figs. 5(a) and 5(b) as a function of the Ni content x, respectively. Both of them diminish with increasing Ni content, in accordance with the gradual suppression of superconductivity as reported in Ref. [22].

It was reported recently that in isostructural $CaK(Fe_{1-x}Ni_x)_4As_4$, the Ni doping may lead to the emergence of a hedgehog-type SVC order of the Fe moments [32,33], which is different from the stripe-type Fe-SDW order observed in "122" family iron pnictides [2,7,35]. However, within our experimental resolution, the proposed recovery of Fe-AFM order with Ni doping cannot be identified at $Q = (0.5, 0.5, L)$ (L = integers), probably due to the weakness of related magnetic reflections from small Fe^{2+} moments and high background in the NPD measurements. Future neutron diffraction experiments on large single-crystal samples of $RbEu(Fe_{1-x}Ni_x)_4As_4$, if available, will be crucial to confirm the possibly restored antiferromagnetism in the Fe sublattice.

The variation of the magnetic structure of Eu in $RbEu(Fe_{1-x}Ni_x)_4As_4$ can be understood semiquantitatively in consideration of the exchange couplings. As the magnetism of Eu in Eu1144 is believed to be of a 2D character, the helix rotation angle θ between the ferromagnetic Eu^{2+} layers predominantly depend on the competition between the nearest (J_{c1}) and next-nearest (J_{c2}) interplayer couplings [see Fig. 6(a)] with $\cos\theta = -\frac{J_{c1}}{4J_{c2}}$ [36]. These exchange couplings between interlayer Eu^{2+} moments are realized through the indirect RKKY interaction J_{RKKY}, mediated by the conduction d electrons on the FeAs layers in the form of $J_c \propto J_{RKKY}\cos(2k_F r)/r^3$, where r denotes the interlayer distance between the Eu^{2+} moments and k_F is the Fermi vector [37–40]. Using first-principles calculations, it is figured out that the RKKY interaction strength J_{RKKY} is isotropic and barely changed upon Ni doping (~0.12 meV) [41]. In the undoped Eu1144, J_{c1} is expected to be zero (for $\theta = 90^\circ$ and $\cos\theta = 0$), consistent with the 2D character of the Eu magnetism. This corresponds to $2k_{F0}r_0 = (2n + 1)\pi/2$ with

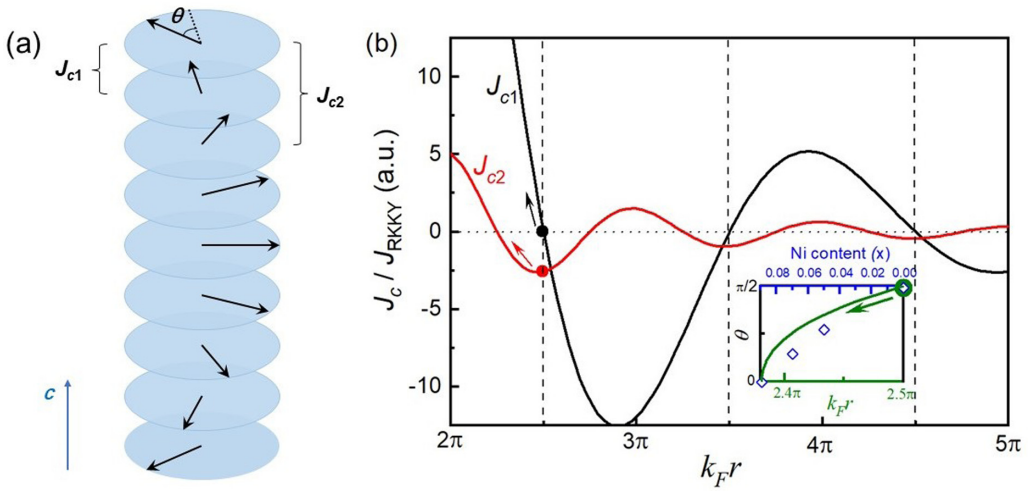

FIG. 6. (a) An illustration of the spin directions in different layers of the helical magnetic structure and (b) a semiquantitative description of the interlayer couplings as well as the rotation angle θ in the helix as a function of $k_F r$. The nearest (J_{c1}, black solid line) and next-nearest (J_{c2}, red solid line) interplayer couplings are assumed to be in the form of $J_{c1} = CJ_{\mathrm{RKKY}}\cos(2k_F r)/r^3$ and $J_{c2} = CJ_{\mathrm{RKKY}}\cos(4k_F r)/(2r)^3$, respectively, where C is a scaling constant. The helix rotation angle θ (in the inset) is then calculated using $\cos\theta = -\frac{J_{c1}}{4J_{c2}}$. The vertical dashed lines in (b) mark the possible $k_F r$ values of undoped Eu1144, where $J_{c1} = 0$ and $J_{c2} < 0$. Assuming that for undoped Eu1144 $k_F r = 2.5\pi$, the black, red, and olive arrows next to the corresponding solid circles represent the shifts of J_{c1}, J_{c2}, and θ values with the decrease in $k_F r$ induced by Ni doping. The blue diamonds in the inset of (b) represent the θ values for different Ni content x determined experimentally as shown in Fig. 5(b) for comparison.

k_{F0} and r_0 being the Fermi vector and nearest interlayer distance between the Eu^{2+} moments without Ni doping. $J_{c2} \propto J_{\mathrm{RKKY}}\cos(4k_{F0}r_0)/(2r_0)^3$ is, therefore, negative, responsible for the antiferromagnetic next-nearest interlayer coupling. As the hole carriers are compensated by the substitution of Ni^{2+} ($3d^8$) for Fe^{2+} ($3d^6$), the Fermi vector k_F shrinks effectively, leading to the decrease in $k_F r$. Therefore, $|J_{c1}|$ increases and $|J_{c2}|$ decreases as the value of $k_F r$ is tuned away from $(n + 1/2)\pi$, resulting in the increase in $\cos\theta$ $(= -\frac{J_{c1}}{4J_{c2}})$ and the decrease in θ as shown in Fig. 6(b) and its inset. This well explains the gradual disappearance of relative rotation between adjacent Eu^{2+} layers with increasing Ni doping as determined experimentally.

It is argued that the emergence of the helical magnetic structure with a period of four unit cells along the c axis in undoped Eu1144 [$k = (0, 0, 0.25)$] is favored by the exchange interaction between superconductivity and ferromagnetism [24] as predicted by Anderson and Suhl a long time ago to be one solution for the compromise between these two antagonistic phenomena [42]. As an alternate scenario, it is proposed theoretically that the ferromagnetic contribution to the interlayer RKKY interaction from the nonsuperconducting normal parts and the antiferromagnetic contribution from the superconducting layers compete with each other, giving rise to the helical ground-state magnetic configuration as a result of frustration [25]. It is worth pointing out that our experimental results are also qualitatively consistent with these arguments. On one hand, the helix rotation angle θ diminishes with Ni doping, thus, releasing the frustration in favor of a collinear ferromagnetic structure. On the other hand, according to the prediction by Anderson and Suhl [42], the periodicity of the spin helix d is correlated with the superconducting coherence length ξ_0 in the form of $d \propto (\xi_0)^{1/3}$ [42]. As the superconducting transition temperature T_{SC} and the upper critical field H_{c2} decrease with increasing Ni doping [23], ξ_0 increases according to the Ginzburg-Landau formalism $H_{c2} = \Phi_0/2\pi{\xi_0}^2$, which is consistent with the diminishing θ and increasing helix periodicity d. Although some recent spectroscopic measurements seem to suggest the decoupling of magnetism from Eu from superconducting FeAs layers [43,44], we note that a recent scanning Hall microscopy experiment has revealed a pronounced suppression of the superfluid density near the Eu magnetic ordering temperature in Eu1144, indicating a pronounced exchange interaction between the superconducting and magnetic subsystems [45].

In conclusion, the magnetic structures of $RbEu(Fe_{1-x}Ni_x)_4As_4$ superconductors are systematically investigated by neutron powder diffraction. It is found that as the superconductivity gets suppressed gradually with the increase in Ni doping, the magnetic propagation vector of the Eu sublattice diminishes, corresponding to the decrease in the rotation angle between the moments in neighboring Eu layers with a helical structure. For nonsuperconducting $RbEu(Fe_{0.91}Ni_{0.09})_4As_4$, all the Eu^{2+} spins point along the tetragonal (1 1 0) direction, forming a purely collinear ferromagnetic structure. Such an evolution from helical to collinear ferromagnetic order of the Eu^{2+} spins with increasing Ni doping is well supported by first-principles calculations. The variation of the rotation angle between adjacent Eu^{2+} layers can be well explained by considering the change in magnetic exchange couplings mediated by the indirect RKKY interaction.

ACKNOWLEDGMENTS

This work was partly based on experiments performed at the Australian Nuclear Science and Technology Organisation (ANSTO), Sydney, Australia and the Institut Laue-Langevin

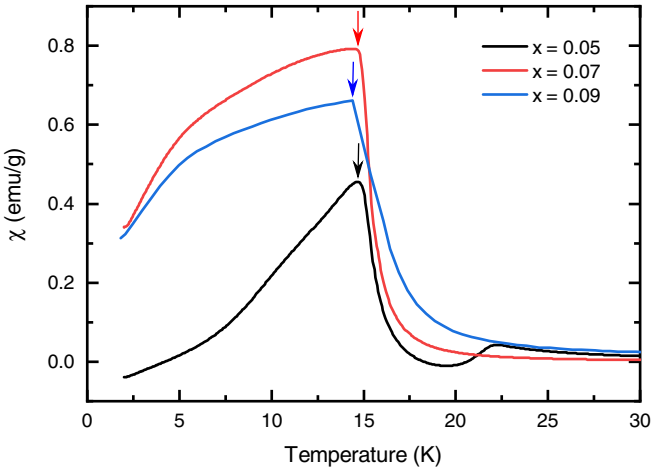

FIG. 7. Temperature dependence of the DC magnetic susceptibility (χ) measured under a magnetic field of 10 Oe in ZFC mode for $RbEu(Fe_{1-x}Ni_x)_4As_4$ with $x = 0.05$, 0.07, and 0.09. The arrows mark the magnetic ordering temperature of the Eu sublattice T_m.

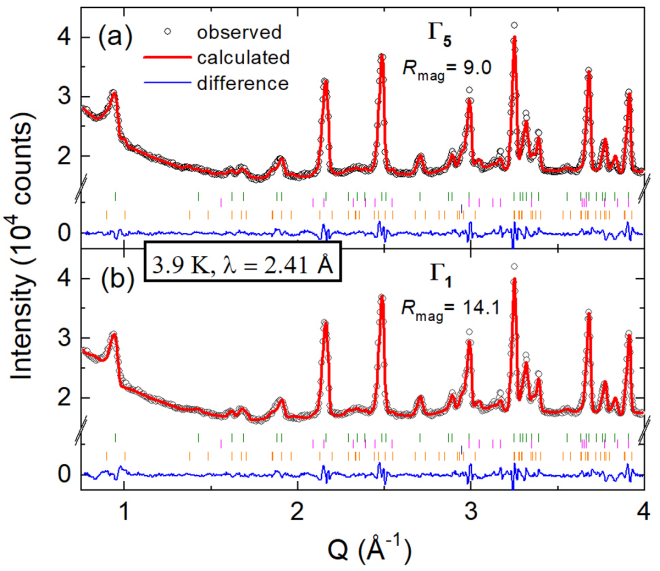

FIG. 8. The fitting results to the higher-resolution NPD patterns of $RbEu(Fe_{0.95}Ni_{0.05})_4As_4$ collected at 3.9 K with $\lambda = 2.41$ Å, adopting the in-plane helical magnetic structure described by (a) Γ_5 and the c-axis spin-density-wave-type magnetic structure described by (b) Γ_1, respectively. The circles represent the observed intensities, and the solid lines are the calculated patterns. The differences between the observed and the calculated intensities are shown at the bottom. The vertical bars in olive, magenta, navy, and orange colors indicate the expected nuclear Bragg reflections from the $RbEu(Fe_{0.95}Ni_{0.05})_4As_4$ main phase, FeAs impurity, vanadium sample container, and the magnetic Bragg reflections from $RbEu(Fe_{0.95}Ni_{0.05})_4As_4$, respectively.

(ILL), Grenoble, France. W.J. acknowledges S. Gao, H. Deng, and K. Friese for helpful discussions. We acknowledge support from the National Natural Science Foundation of China (Grants No. 12074023 and No. 11927807), the National Key Research and Development Program of China (Grant No. 2016YFA0300202), the Fundamental Research Funds for the Central Universities in China, and Shanghai Science and Technology Committee (Grants No. 19ZR1402600 and No. 20DZ1100604).

APPENDIX A: DC MAGNETIC SUSCEPTIBILITY

Figure 7 shows the DC magnetic susceptibility (χ) of the polycrystalline $RbEu(Fe_{1-x}Ni_x)_4As_4$ with $x = 0.05$, 0.07, and 0.09, measured under an applied magnetic field of 10 Oe in the zero-field-cooling (ZFC) mode. The sample with $x = 0.05$ displays clearly a diamagnetic response at ~22 K, evidencing a superconducting transition as expected for a ferromagnetic superconductor. In contrast, the other two samples do not show the diamagnetic response due to the absence of the Meissner effect as expected for a superconducting ferromagnet ($x = 0.07$) or a nonsuperconductor ($x = 0.09$). The magnetic ordering temperature of the Eu sublattice T_m as determined from the peak position in the ZFC curve decreases from ~14.8(1) K for $x = 0.05$ and $x = 0.07$ to ~14.6(2) K for $x = 0.09$. The $\chi(T)$ behaviors of all three samples and the tendency of variation of T_m with the Ni-doping level are well consistent with the results reported in Ref. [22] for the same compositions.

TABLE IV. Basis vectors of the IRs for the Eu atoms in $RbEu(Fe_{0.95}Ni_{0.05})_4As_4$ with space group $P4/mmm$ and $k = (0, 0, 0.136)$, obtained from representation analysis. The Eu atoms occupy the $1a$ sites. The magnetic R values (R_{mag}) of the fitting for each IR is listed.

IRs	R_{mag}	ψ_ν	Components	Eu
Γ_1^1	14.1	ψ_1	Real	(0, 0, 1)
Γ_5^2	9.0	ψ_1	Real	(1, 0, 0)
			Imaginary	(0, −1, 0)
		ψ_2	Real	(1, 0, 0)
			Imaginary	(0, 1, 0)

APPENDIX B: MAGNETIC SYMMETRY ANALYSIS AND MODEL SELECTION

Magnetic symmetry analysis was performed using the BASIREPS program integrated in the FULLPROF suite.

For $RbEu(Fe_{0.95}Ni_{0.05})_4As_4$ with the space-group $P4/mmm$ and $k = (0, 0, 0.136)$, the magnetic representation Γ_{mag} for the Eu ($1a$) site can be decomposed as the sum of two irreducible representations (IRs), whose basis vectors are listed in Table IV,

$$\Gamma_{mag} = \Gamma_1^1 \oplus \Gamma_5^2.$$

Γ_1 allows the c-axis aligned ferromagnetic Eu layers stacking with modulated moment size values at different layers. On the other hand, Γ_5 allows the in-plane aligned ferromagnetic Eu layers to stack helically along the c axis with a constant moment size value at different layers, which yields a smaller magnetic R values (R_{mag}) and a better agreement with the intensities in the very low-Q region where the magnetic form factor dominates in the fitting to the NPD pattern at 3.9 K as

TABLE V. Basis vectors of the IRs for the Eu atoms in $RbEu(Fe_{0.91}Ni_{0.09})_4As_4$ with space group $P4/mmm$ and $k = 0$, obtained from representation analysis. The Eu atoms occupy the $1a$ sites. The magnetic R values (R_{mag}) of the fitting for each IR is listed.

IRs	R_{mag}	ψ_ν	Components	Eu
Γ_8^1	17.1	ψ_1	Real	(0, 0, 1)
Γ_9^2	8.0	ψ_1	Real	(0, 1, 0)
		ψ_2	Real	(1, 0, 0)

shown in Fig. 8. In addition, the magnetic structure described by Γ_1 with the modulated moments aligned along the c axis is not consistent with the easy-plane magnetization as reported by Willa *et al.* in Ref. [23], and it yields unrealistic moment values as large as $\sim 8\,\mu_B$ for certain Eu sites with a total spin of $S = 7/2$.

For $RbEu(Fe_{0.91}Ni_{0.09})_4As_4$ with the space-group $P4/mmm$ and $k = 0$, the magnetic representation Γ_{mag} for the Eu ($1a$) site can also be decomposed as the sum of two IRs, whose basis vectors are listed in Table V,

$$\Gamma_{mag} = \Gamma_8^1 \oplus \Gamma_9^2.$$

They correspond to the collinear ferromagnetic structures in which the Eu^{2+} moments are aligned along the c axis and on the ab plane, respectively. The moment direction of Eu^{2+} spins can be preidentified according to the nature of magnetic neutron diffraction. As the magnetic scattering is only sensitive to the component of the moment perpendicular to Q, dramatic enhancements of intensities of ($0\ 0\ L$) peaks (see Fig. 3) and no visible changes in ($H\ K\ 0$) peak intensities suggest that the Eu^{2+} moments are mostly lying on the ab plane so that the magnetic-structure model described by Γ_8 can be excluded. Indeed the Γ_9 model with the Eu^{2+} spins aligned ferromagnetically on the ab plane fits the diffraction patterns better with smaller magnetic R values (R_{mag}).

APPENDIX C: .CIF AND .MCIF FILES

The .cif and .mcif files, containing the crystallographic and magnetic symmetry information of all three samples generated by FULLPROF are enclosed.

[1] Y. Kamihara, T. Watanabe, M. Hirano, and H. Hosono, Iron-based layered superconductor $La[O_{1-x}F_x]FeAs$ with $T_c = 26$ K, J. Am. Chem. Soc. **130**, 3296 (2008).

[2] P. Dai, Antiferromagnetic order and spin dynamics in iron-based superconductors, Rev. Mod. Phys. **87**, 855 (2015).

[3] S. Zapf and M. Dressel, Europium-based iron pnictides: a unique laboratory for magnetism, superconductivity and structural effects, Rep. Prog. Phys. **80**, 016501 (2017).

[4] Y. Xiao, Y. Su, W. Schmidt, K. Schmalzl, C. M. N. Kumar, S. Price, T. Chatterji, R. Mittal, L. J. Chang, S. Nandi, N. Kumar, S. K. Dhar, A. Thamizhavel, and T. Brueckel, Field-induced spin reorientation and giant spin-lattice coupling in $EuFe_2As_2$, Phys. Rev. B **81**, 220406(R) (2010).

[5] Y. Xiao, Y. Su, S. Nandi, S. Price, B. Schmitz, C. M. N. Kumar, R. Mittal, T. Chatterji, N. Kumar, S. K. Dhar *et al.*, Anomalous in-plane magnetoresistance in a $EuFe_2As_2$ single crystal: Evidence of strong spin-charge-lattice coupling, Phys. Rev. B **85**, 094504 (2012).

[6] Z. Ren, Z. Zhu, S. Jiang, X. Xu, Q. Tao, C. Wang, C. Feng, G. Cao, and Z. Xu, Antiferromagnetic transition in $EuFe_2As_2$: A possible parent compound for superconductors, Phys. Rev. B **78**, 052501 (2008).

[7] Y. Xiao, Y. Su, M. Meven, R. Mittal, C. M. N. Kumar, T. Chatterji, S. Price, J. Persson, N. Kumar, S. K. Dhar *et al.*, Magnetic structure of $EuFe_2As_2$ determined by single-crystal neutron diffraction, Phys. Rev. B **80**, 174424 (2009).

[8] Z. Ren, Q. Tao, S. Jiang, C. Feng, C. Wang, J. Dai, G. Cao, and Z. Xu, Superconductivity Induced by Phosphorus Doping and Its Coexistence with Ferromagnetism in $EuFe_2(As_{0.7}P_{0.3})_2$, Phys. Rev. Lett. **102**, 137002 (2009).

[9] C. F. Miclea, M. Nicklas, H. S. Jeevan, D. Kasinathan, Z. Hossain, H. Rosner, P. Gegenwart, C. Geibel, and F. Steglich, Evidence for a reentrant superconducting state in $EuFe_2As_2$ under pressure, Phys. Rev. B **79**, 212509 (2009).

[10] W. T. Jin, S. Nandi, Y. Xiao, Y. Su, O. Zaharko, Z. Guguchia, Z. Bukowski, S. Price, W. H. Jiao, G. H. Cao *et al.*, Magnetic structure of superconducting $Eu(Fe_{0.82}Co_{0.18})_2As_2$ as revealed by single-crystal neutron diffraction, Phys. Rev. B **88**, 214516 (2013).

[11] S. Nandi, W. T. Jin, Y. Xiao, Y. Su, S. Price, D. K. Shukla, J. Strempfer, H. S. Jeevan, P. Gegenwart, and T. Brückel, Coexistence of superconductivity and ferromagnetism in P-doped $EuFe_2As_2$, Phys. Rev. B **89**, 014512 (2014).

[12] W. T. Jin, W. Li, Y. Su, S. Nandi, Y. Xiao, W. H. Jiao, M. Meven, A. P. Sazonov, E. Feng, Y. Chen *et al.*, Magnetic ground state of superconducting $Eu(Fe_{0.88}Ir_{0.12})_2As_2$: A combined neutron diffraction and first-principles calculation study, Phys. Rev. B **91**, 064506 (2015).

[13] Z. Zhou, W. T. Jin, W. Li, S. Nandi, B. Ouladdiaf, Z. Yan, X. Wei, X. Xu, W. H. Jiao, N. Qureshi *et al.*, Universal critical behavior in the ferromagnetic superconductor $Eu(Fe_{0.75}Ru_{0.25})_2As_2$, Phys. Rev. B **100**, 060406(R) (2019).

[14] W. T. Jin, J. P. Sun, G. Z. Ye, Y. Xiao, Y. Su, K. Schmazl, S. Nandi, Z. Bukowski, Z. Guguchia, E. Feng *et al.*, Hydrostatic pressure effects on the static magnetism in $Eu(Fe_{0.925}Co_{0.075})_2As_2$, Sci. Rep. **7**, 3532 (2017).

[15] A. Iyo, K. Kawashima, T. Kinjo, T. Nishio, S. Ishida, H. Fujihisa, Y. Gotoh, K. Kihou, H. Eisaki, and Y. Yoshida, New-structure-type fe-based superconductors: $CaAFe_4As_4$ (A = K, Rb, Cs) (A = K, Rb, Cs) and $SrAFe_4As_4$ (A = Rb, Cs), J. Am. Chem. Soc. **138**, 3410 (2016).

[16] Z. Bukowski, S. Weyeneth, R. Puzniak, J. Karpinski, and B. Batlogg, Bulk superconductivity at 2.6 K in undoped $RbFe_2As_2$, Physica C **470**, S328 (2010).

[17] Y. Liu, Y.-B. Liu, Z.-T. Tang, H. Jiang, Z.-C. Wang, A. Ablimit, W.-H. Jiao, Q. Tao, C.-M. Feng, Z.-A. Xu *et al.*, Superconductivity and ferromagnetism in hole-doped $RbEuFe_4As_4$, Phys. Rev. B **93**, 214503 (2016).

[18] M. P. Smylie, K. Willa, J.-K. Bao, K. Ryan, Z. Islam, H. Claus, Y. Simsek, Z. Diao, A. Rydh, A. E. Koshelev *et al.*, Anisotropic superconductivity and magnetism in single-crystal $RbEuFe_4As_4$, Phys. Rev. B **98**, 104503 (2018).

[19] K. Iida, Y. Nagai, S. Ishida, M. Ishikado, N. Murai, A. D. Christianson, H. Yoshida, Y. Inamura, H. Nakamura, A. Nakao *et al.*, Coexisting spin resonance and long-range magnetic order of Eu in $EuRbFe_4As_4$, Phys. Rev. B **100**, 014506 (2019).

[20] X. Tan, G. Fabbris, D. Haskel, A. A. Yaroslavtsev, H. Cao, C. M. Thompson, K. Kovnir, A. P. Menushenkov, R. V. Chernikov, V. Ovidiu Garlea *et al.*, A transition from localized to strongly correlated electron behavior and mixed valence driven by physical or chemical pressure in ACo_2As_2 (A = Eu and Ca), J. Am. Chem. Soc. **138**, 2724 (2016).

[21] W. T. Jin, N. Qureshi, Z. Bukowski, Y. Xiao, S. Nandi, M. Babij, Z. Fu, Y. Su, and T. Brückel, Spiral magnetic ordering of the Eu moments in $EuNi_2As_2$, Phys. Rev. B **99**, 014425 (2019).

[22] Y. Liu, Y.-B. Liu, Y.-L. Yu, Q. Tao, C.-M. Feng, and G.-H. Cao, $RbEu(Fe_{1-x}Ni_x)_4As_4$: From a ferromagnetic superconductor to a superconducting ferromagnet, Phys. Rev. B **96**, 224510 (2017).

[23] K. Willa, M. P. Smylie, Y. Simsek, J.-K. Bao, D. Y. Chung, M. G. Kanatzidis, W.-K. Kwok, and U. Welp, Magnetic and superconducting anisotropy in Ni-doped $RbEuFe_4As_4$ single crystals, Phys. Rev. B **101**, 064508 (2020).

[24] Z. Devizorova and A. Buzdin, Superconductivity-driven helical magnetic structure in $EuRbFe_4As_4$ ferromagnetic superconductor, Phys. Rev. B **100**, 104523 (2019).

[25] A. E. Koshelev, Helical structures in layered magnetic superconductors due to indirect exchange interactions mediated by interlayer tunneling, Phys. Rev. B **100**, 224503 (2019).

[26] A. J. Studer, M. E. Hagen, and T. J. Noakes, Wombat: The high-intensity powder diffractometer at the OPAL reactor, Phyica B **385-386**, 1013 (2006).

[27] J. Rodriguez-Carvajal, Recent advances in magnetic structure determination by neutron powder diffraction, Physica B **192**, 55 (1993).

[28] P. E. Blöchl, Projector augmented-wave method, Phys. Rev. B **50**, 17953 (1994).

[29] G. Kresse and J. Furthmüller, Efficient iterative schemes for ab initio total-energy calculations using a plane-wave basis set, Phys. Rev. B **54**, 11169 (1996).

[30] J. P. Perdew, K. Burke, and M. Ernzerhof, Generalized Gradient Approximation Made Simple, Phys. Rev. Lett. **77**, 3865 (1996).

[31] W. Li, J. X. Zhu, Y. Chen, and C. S. Ting, First-principles calculations of the electronic structure of iron-pnictide $EuFe_2(As, P)_2$ superconductors: Evidence for antiferromagnetic spin order, Phys. Rev. B **86**, 155119 (2012).

[32] W. R. Meier, Q.-P. Ding, A. Kreyssig, S. L. Bud'ko, A. Sapkota, K. Kothapalli, V. Borisov, R. Valentí, C. D. Batista, P. P. Orth *et al.*, Hedgehog spin-vortex crystal stabilized in a hole-doped iron-based superconductor, npj Quantum Mater. **3**, 5 (2018).

[33] A. Kreyssig, J. M. Wilde, A. E. Böhmer, W. Tian, W. R. Meier, B. Li, B. G. Ueland, M. Xu, S. L. Bud'ko, P. C. Canfield *et al.*, Antiferromagnetic order in $CaK(Fe_{1-x}Ni_x)_4As_4$ and its interplay with superconductivity, Phys. Rev. B **97**, 224521 (2018).

[34] M. I. Aroyo, J. M. Perez-Mato, D. Orobengoa, E. Tasci, G. de la Flor, and A. Kirov, Crystallography online: Bilbao Crystallographic Server, Bulg. Chem. Commun. **43**, 183 (2011).

[35] Y. Su, P. Link, A. Schneidewind, T. Wolf, P. Adelmann, Y. Xiao, M. Meven, R. Mittal, M. Rotter, D. Johrendt *et al.*, Antiferromagnetic ordering and structural phase transition in $Ba_2Fe_2As_2$ with Sn incorporated from the growth flux, Phys. Rev. B **79**, 064504 (2009).

[36] S. Blundell, *Magnetism in Condensed Matter* (Oxford University Press, Oxford, 2001).

[37] M. A. Ruderman and C. Kittel, Indirect exchange coupling of nuclear magnetic moments by conduction electrons, Phys. Rev. **96**, 99 (1954).

[38] T. Kasuya, A theory of metallic ferro- and antiferromagnetism on zener's model, Prog. Theor. Phys. **16**, 45 (1956).

[39] K. Yosida, Magnetic properties of Cu-Mn alloys, Phys. Rev. **106**, 893 (1957).

[40] A. Akbari, P. Thalmeier, and I. Eremin, Evolution of the multiband Ruderman-Kittel-Kasuya-Yosida interaction: application to iron pnictides and chalcogenides, New J. Phys. **15**, 033034 (2013).

[41] C. Xu, Q. Chen, and C. Cao, Unique crystal field splitting and multiband RKKY interactions in Ni-doped$EuRbFe_4As_4$, Commun. Phys. **2**, 16 (2019).

[42] P. W. Anderson and H. Suhl, Spin alignment in the superconducting state, Phys. Rev. **116**, 898 (1959).

[43] M. Hemmida, N. Winterhalter-Stocker, D. Ehlers, H.-A. K. von Nidda, M. Yao, J. Bannies, E. D. L. Rienks, R. Kurleto, C. Felser, B. Büchner *et al.*, Topological magnetic order and superconductivity in $EuRbFe_4As_4$, Phys. Rev. B **103**, 195112 (2021).

[44] T. K. Kim, K. S. Pervakov, D. V. Evtushinsky, S. W. Jung, G. Poelchen, K. Kummer, V. A. Vlasenko, A. V. Sadakov, A. S. Usoltsev, V. M. Pudalov *et al.*, Electronic structure and coexistence of superconductivity with magnetism in $RbEuFe_4As_4$, Phys. Rev. B **103**, 174517 (2021).

[45] D. Collomb, S. J. Bending, A. E. Koshelev, M. P. Smylie, L. Farrar, J.-K. Bao, D. Y. Chung, M. G. Kanatzidis, W.-K. Kwok, and U. Welp, Observing the Suppression of Superconductivity in $RbEuFe_4As_4$ by Correlated Magnetic Fluctuations, Phys. Rev. Lett. **126**, 157001 (2021).